New Journal of Physics
The open access journal at the forefront of physics

Deutsche Physikalische Gesellschaft DPG IOP Institute of Physics

Measuring the temperature and heating rate of a single ion by imaging

New Journal of Physics
The open access journal at the forefront of physics

Deutsche Physikalische Gesellschaft DPG
IOP Institute of Physics

Published in partnership with: Deutsche Physikalische Gesellschaft and the Institute of Physics

OPEN ACCESS

RECEIVED
24 May 2019

REVISED
16 September 2019

ACCEPTED FOR PUBLICATION
18 October 2019

PUBLISHED
6 November 2019

PAPER

Measuring the temperature and heating rate of a single ion by imaging

Bharath Srivathsan[1,2,3], **Martin Fischer**[1,2], **Lucas Alber**[1,2], **Markus Weber**[1,2], **Markus Sondermann**[1,2] and **Gerd Leuchs**[1,2,4]

[1] Friedrich-Alexander-Universität Erlangen-Nürnberg (FAU), Department of Physics, Staudtstr. 7/B2, D-91058, Erlangen, Germany
[2] Max Planck Institute for the Science of Light, Staudtstr. 2, D-91058, Erlangen, Germany
[3] Centre for Cold Matter, Blackett Laboratory, Imperial College London, Prince Consort Road, London SW7 2AZ, United Kingdom
[4] Department of Physics, University of Ottawa, Ottawa, Ont. K1N 6N5, Canada

E-mail: markus.sondermann@fau.de

Keywords: trapped ions, imaging, temperature, parabolic mirror

Abstract

We present a technique based on high resolution imaging to measure the absolute temperature and the heating rate of a single ion trapped at the focus of a deep parabolic mirror. We collect the fluorescence light scattered by the ion during laser cooling and image it onto a camera. Accounting for the size of the point-spread function and the magnification of the imaging system, we determine the spatial extent of the ion, from which we infer the mean phonon occupation number in the trap. Repeating such measurements and varying the power or the detuning of the cooling laser, we determine the heating rate induced by any kind of effect other than photon scattering. In contrast to other established schemes for measuring the heating rate, the ion is always maintained in a state of thermal equilibrium at temperatures close to the Doppler limit.

1. Introduction

In many atomic physics and quantum optics experiments, the temperature of the atoms under investigation plays a critical role [1–6]. From fundamental tests to quantum information applications, cooling the atoms to ultra-low temperatures has become a prerequisite. To this end, laser cooling and trapping of atoms has become an indispensable tool in many labs. Furthermore, measuring the temperature of the cold atoms becomes important, for instance to understand the physics of the cooling mechanism, or to disclose additional sources of heating and thermal decoherence in the experiment. Depending on the type of the trapping and cooling method employed, several thermometry techniques have been developed.

In the case of trapped ions, the most common way to determine the temperature is to measure the sideband absorption spectrum [7, 8]. This technique requires the ion to be cooled close to the motional ground state of the trap, and therefore is used in combination with ground state cooling schemes such as Raman sideband cooling [9] or cooling employing electromagnetically induced transparency (EIT) [10]. Outside the resolved sideband regime, various techniques exist. One way is to measure the Doppler broadening of the atomic transition due to the motion of the ion [11, 12]. The accuracy of this approach relies on the ability to distinguish the Lorentzian spectrum of an atomic transition from the Gaussian spectrum. The Doppler broadening at sub-mK temperatures is small compared to the natural linewidth of the typically used transitions. Therefore, the statistical uncertainties in data evaluation prevent an accurate determination of the temperature close to the Doppler limit. Particularly, in the Lamb–Dicke Regime the first order Doppler effect is suppressed, and only the higher order Doppler shifts that are much weaker can be observed [13, 14].

In order to enable fast and accurate determination of the temperature of a trapped ion at mK temperatures, thermometry by imaging the spatial extent of an ion has been demonstrated [15–18]. The accuracy of this method was limited only by the imaging resolution and the images' signal-to-noise ratio. In this article, we present the thermometry measurement of a single ion by imaging via a deep parabolic mirror. Our improved

resolution and high collection efficiency [19] allows us to determine the absolute temperature close to the Doppler limit more accurately in comparison to previous demonstrations of this technique. Furthermore, it opens up the possibility to measure temperatures below the Doppler limit, which has until now been possible only by the resolved sideband method or by similarly involved methods such as the one based on interference of fluorescence photons [20]. The high photon collection efficiency of our parabolic-mirror based set-up envisions the application of our method also for cooling processes in which only few photons are scattered, like e.g. EIT cooling.

In addition to the absolute temperature, the heating rate is another important figure of merit in thermometry of trapped ions [21, 22]. In the resolved sideband regime, sideband thermometry is generally employed to measure the heating rate. Outside this regime, the heating rate is traditionally measured from the time-resolved fluorescence rate of the ion during the Doppler cooling process [23]. A similar technique combining the imaging approach and the time-resolved scattering method to determine the heating rate was recently demonstrated [24]. Both these techniques involve heating up the ion to temperatures at-least a few orders of magnitude above the Doppler limit, and therefore depend on several simplifying assumptions about the system. We present an alternative way to determine the heating rate of a single ion employing the imaging approach while varying the cooling laser power or its detuning. The advantage of our technique is that for every measurement point the ion is maintained in a state of thermal equilibrium during the entire measurement sequence. As detailed below, when varying the cooling laser power the effect of a finite heating rate is most evident at low powers, i.e. at low Rabi frequencies and hence low photon scattering rates. Here we again benefit from the collection efficiency of our setup which enables the acquisition of images with sufficient signal-to-noise ratio even from faint light sources.

2. Theory

The temperature T of an ion in an harmonic trap under weak confinement conditions can be approximated as $T \approx \bar{n}\hbar\omega/k_B$, where $\bar{n}$ is the average excitation number of the harmonic oscillator, ω is the trap frequency and k_B is the Boltzmann constant [17]. $\bar{n}$ in turn is related to the rms spread σ_i of the ion in position space as

$$\sigma_i = \sqrt{\frac{\hbar}{2m\omega}(2\bar{n} + 1)}, \tag{1}$$

where m is mass of the ion. In the experiment, we measure σ_i by imaging the ion, and thereby determine $\bar{n}$ and T.

In order to determine the heating rate ζ induced by external factors, we use a simple model of laser cooling [25] which neglects additional heating or cooling due to micromotion. Since micromotion is well compensated in our experiment, this model is well suited to describe the cooling process. Cooling as well as heating induced by interaction of the ion with the cooling light is governed by scattering of photons from the near-resonant cooling beam. The steady state scattering rate of these photons is given by $\Gamma \cdot \rho_{ee}$, where Γ is the spontaneous emission rate of the cooling transition and $\rho_{ee} = \Omega^2/(4\Delta^2 + \Gamma^2 + 2\Omega^2)$ is the steady state excitation of the ion. Δ is the detuning of the laser from the atomic resonance and Ω is the Rabi frequency. Particles confined in harmonic traps can have anisotropic temperature, depending on the angle made by the cooling beam with the trap axes [16]. To include this effect in our model, we define an effective k-vector, $|\vec{k}_{\text{eff}}| = |\vec{k}| \cos\alpha$, where α is the angle made by the cooling laser with a trap axis. The cooling rate along the chosen trap axis is given by

$$\dot{E}_c = -\frac{8\hbar|\vec{k}_{\text{eff}}|^2\Delta\Gamma}{\Omega^2}\frac{k_B T}{m}\rho_{ee}^2. \tag{2}$$

The heating rate during the final stages of Doppler cooling can be approximated as

$$\dot{E}_h = \frac{\rho_{ee}\,\Gamma}{2m}[\hbar^2|\vec{k}_{\text{eff}}|^2 + \xi\,\hbar^2|\vec{k}|^2] + \zeta. \tag{3}$$

The first term in the brackets corresponds to the momentum change along the trap axis due to absorption of a photon, while the second term corresponds to the momentum change due to spontaneous emission along this direction. ξ is a geometry factor that originates from the spatial emission characteristics of the scattered photons. In our experiment, we use a $J = 1/2$ to $J = 1/2$ transition with a nearly isotropic emission pattern. Therefore, we use a geometry factor of $\xi = 1/3$. In addition, we use a constant factor ζ to include any kind of heating other than photon scattering of the cooling light in the model.

The equilibrium temperature is reached when the heating and cooling rates are equal: $\dot{E}_c + \dot{E}_h = 0$. Below, we will measure σ_i while either varying Ω or Δ. In both cases, we will obtain ζ by fitting our model to the experimental data.

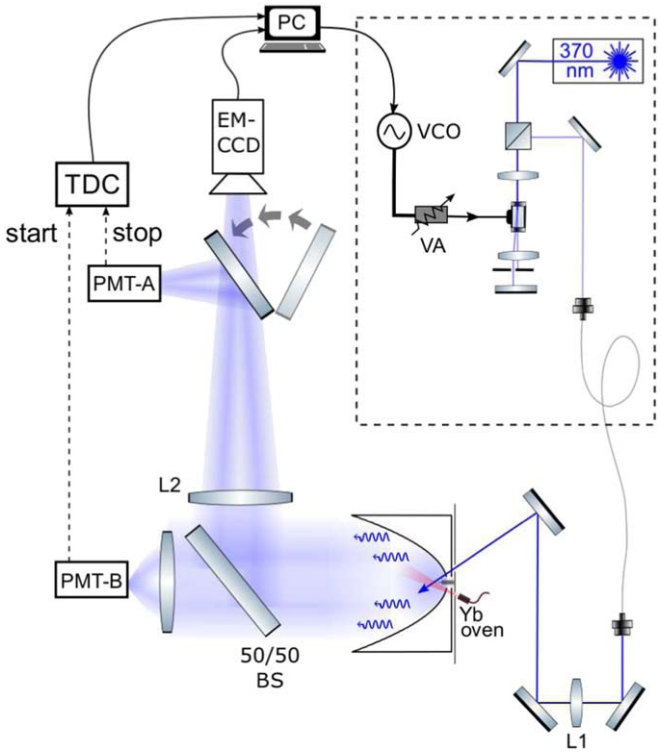

Figure 1. Schematic of our experimental setup. A stylus ion trap is used to trap a single $^{174}Yb^{+}$ at the focus of a deep parabolic mirror (PM).

3. Experiment

The schematic of our experimental setup is shown in figure 1. We trap a single $^{174}Yb^{+}$ ion in the focal region of a deep parabolic mirror using a stylus like ion trap [26]. The trap is driven with a radio frequency (RF) signal at $\Omega_{RF} = 2\pi \cdot 5.2$ MHz and an amplitude of 1 kV. The distance of the ion to the closest electrode is estimated to be $\gtrsim$300 μm. Excess micromotion is compensated using a set of four electrodes [26] reducing residual electric fields to magnitudes below 0.45 ± 0.08 V m^{-1}.

The trap is mounted on a *XYZ* piezo translation stage (PIHera P-622K058) with a positioning accuracy of about $\pm$1 nm. With the aid of the piezo stage, the ion can be positioned and scanned in all three directions around the focal point of the mirror. A 370 nm frequency doubled diode laser (Toptica) is used for Doppler cooling the ion. The ion is repumped from the metastable $D_{3/2}$ state with a diode laser (Toptica) at a wavelength of 935 nm. The detuning of the lasers is set by using 200 MHz Accusto-Optic-Modulators (AOM), aligned in 'double-pass' configuration, and driven by the amplified signal of a Voltage Controlled Oscillator (VCO). The lasers are stabilized to a frequency comb (Toptica DFC). The frequency shifted beams are coupled into polarization maintaining single mode optical fibers, and focused onto the ion using a 400 mm focal length lens (L1). The optical power of the cooling beam can be tuned by varying the RF power supplied to the AOM using a Variable attenuator (VA). The parabolic mirror (focal length of 2.1 mm) collimates the fluorescence light scattered by the ion, and acts as an objective for our imaging system. The mirror covers 82% of a 4π solid angle, i.e. it collects 82% of the photons radiated by an isotropic emitter [19], neglecting the aluminum mirror's finite reflectivity of 0.9. A 300 mm focal-length lens (L2) along with a one-to-one telescope using lenses of focal length 50 mm (not shown in figure 1) is used to image the ion on an electron-multiplying charge-coupled device (EM-CCD) camera (Princeton Instruments PhotonMAX 512B) with a pixel size of 16 μm. A flip mirror (FM) directs the fluorescence photons instead to a Photo-Multiplier-Tube (PMT-A). The trap frequencies were measured to be 205 and 196 kHz in the lateral directions (*X* and *Y*), and 390 kHz in the axial direction (*Z*) by applying AC fields to one of the trap electrodes. The cooling beam has an angle α of 71° with both the lateral trap axes.

As introduced above, we measure the temperature of the ion by determining the width of the image recorded on the EM-CCD camera. Due to the geometry of the trap electrodes (see [19]), the lateral trap axes make an angle of 45° with respect to the edges of the pixel array of the camera. Therefore, we rotate the images by nearest

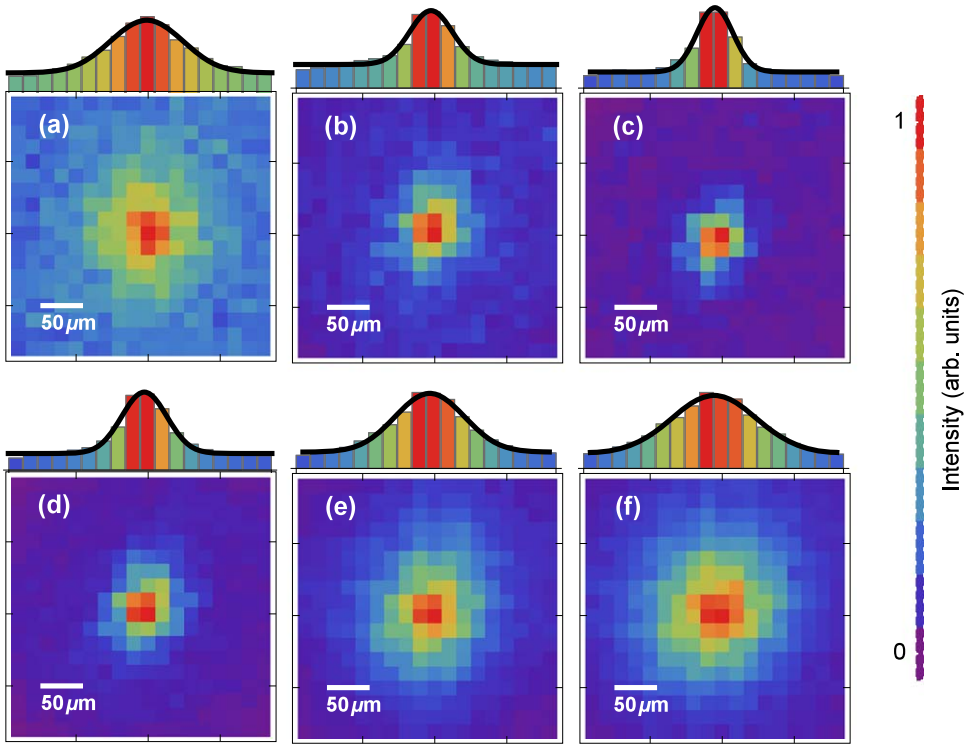

Figure 2. Images of the single ion on the EM-CCD camera for Rabi frequencies Ω of (a) 0.012 Γ, (b) 0.025 Γ, (c) 0.23 Γ, (d) 1.1 Γ, (e) 2.4 Γ, and (f) 3.3 Γ. The pixel sum along the columns is shown as bars above each image. The solid (black) line shows the corresponding Gaussian fits used to determine the image width along this direction, σ. The color scale is normalized to the maximum intensity observed in each image, respectively. All images are recorded at a detuning $\Delta = -2\pi \times 13$ MHz.

neighbor interpolation to make the pixel array axis coincide with the trap axis[5]. For simplicity, we restrict the discussion to one spatial dimension.

First, we project the image onto the horizontal direction by summing over all pixels in each column. We then determine the rms image width σ from this projection by using a 1D Gaussian fit. The image recorded on the camera is a convolution of the imaging point-spread function (PSF) and the 'true image' of the ion. Assuming both the PSF and the true image to be Gaussian spots, the width of the recorded image can be approximated as

$$\sigma = \sqrt{\sigma_{\mathrm{PSF}}^2 + M^2\sigma_i^2}. \tag{4}$$

In order to determine the temperature of the ion, we need to extract σ_i from the measured σ. For this process the magnification M of the imaging system as well as the width σ_{PSF} of the imaging PSF need to be known. M is measured by moving the ion in lateral directions, and measuring the image shift on the camera as outlined in appendix A, yielding $M = 113 \pm 2$. We use σ_{PSF} as a free parameter in the fitting procedure discussed below.

Several example images acquired at different Rabi frequencies Ω are shown in figure 2. The Rabi frequency is obtained by one calibration measurement at fixed power (see appendix D). All other values of Ω are then calculated from the power of the cooling laser and the power used in the calibration measurement. As expected, the width of the images in figure 2 varies with the Rabi frequency Ω.

We now turn to the determination of the heating rate ζ. We fit our model to a set of image widths σ by varying either Ω at fixed Δ or vice versa. The free fit parameters are ζ and σ_{PSF}. The result of the measurement and the fit for varying Ω at a fixed detuning $\Delta/2\pi = -13$ MHz are shown in figure 3. The increase of the image width and thus the ion temperature at very small Rabi frequencies indicates a non-zero excess heating. Here, the number of photon scattering events is too small to compensate for non-radiative heating processes. On the contrary, in the absence of such heating processes the spatial spread of the ion and hence the measured image width would remain at a low value also for Rabi frequencies approaching zero. Moreover, the smaller the heating rate the smaller will be the increase of the ion's spatial width and the smaller will be the Rabi frequency at which this increase may become recognizable. Therefore, the determination of low heating rates benefits from imaging optics with large collection efficiency.

The lowest Rabi frequency investigated in figure 3 corresponds to a saturation parameter of 3×10^{-4}. For the life time of the excited state of the cooling transition (8.1 ns) and the used detuning this corresponds to about

[5] We use MATLAB *imrotate* function to rotate the images.

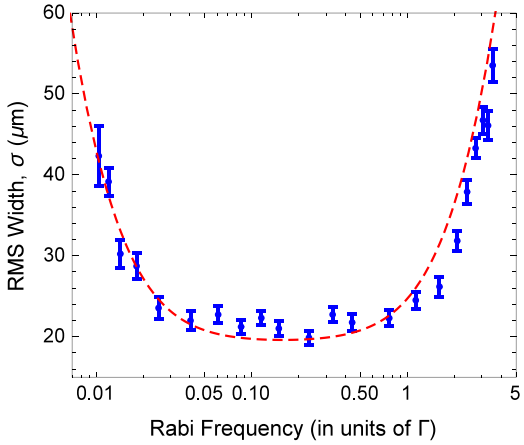

Figure 3. Image rms width along the horizontal direction as a function of Rabi frequency Ω at a fixed detuning of $\Delta/2\pi = -13$ MHz. Error bars represent the uncertainty of the image width obtained by fitting a Gaussian to the camera images. The dashed (red) line represents a fit to the model described in the text. The only free parameters used in the fit are the heating rate ζ and the width of the PSF of the imaging system $\sigma_{\rm PSF}$. The obtained value of ζ is 0.38 ± 0.07 quanta ms^{-1}.

6.5×10^3 photons per second *scattered into the full solid angle*. In view of inevitable losses in any practical detection beam path, the above number underlines the necessity of imaging optics covering a large fraction of the solid angle.

The heating rate as determined from the fit shown in figure 3 is 0.38 ± 0.07 quanta ms^{-1}. The width of the imaging PSF is $\sigma_{\rm PSF} = 6.6 \pm 2.7$ μm, which is in good agreement with the expected PSF of 7.1 μm determined from simulations including the interferometrically measured aberrations of our parabolic mirror [27] (see appendix C). The average phonon number $\bar{n}$ and thus the temperature of the ion for any Ω can now be determined using these parameters.

The lowest measured σ_i is 0.166 ± 0.013 μm, for a Rabi frequency of $\Omega = 0.23\,\Gamma$. This corresponds to a mean phonon occupation number $\bar{n}$ of 97 ± 15, and a temperature of 950 ± 147 μK. In the Doppler limit, the temperature according to $k_{\rm B}T \approx \hbar\Gamma/2$ is expected to be about $T_{\rm D} = 470$ μK. Thus, the temperature of the ion is found to be about twice this Doppler limit, mainly due to a large angle between the cooling beam and the trap axis.

Recalling the finite amount of excess micromotion one could argue that the measured spatial width of the ion is enlarged in comparison to the prediction of a Doppler cooled harmonic oscillator. As detailed in appendix B, this contribution can be estimated to be not larger than 8.3 ± 1.5 nm. This value is far below the smallest measured size and therefore neglected. Similarly, the effects of a time-dependent trapping potential have been shown to enlarge the ion's spatial spread by about only 5% for trap parameters comparable to the ones used here [28].

Furthermore, it can be seen that for the measured temperatures, the contribution of the PSF ($\sigma_{\rm PSF}$) to the measured image width (σ) is much smaller than the contribution from spatial extent of the ion wavefunction (σ_i). Hence, this method can be used for measuring even lower temperatures. From the standard error estimates of $\sigma_{\rm PSF}$ and M, we estimate the minimum measurable temperature with a 50% relative error to be $\approx$200 μK[6], which is well below the standard Doppler limit.

An alternative way to measure the heating rate of the ion is to measure σ when varying the detuning Δ. We fix the cooling beam power such that $\Omega = 0.2\,\Gamma$. The detuning is varied by using the VCO, and the image width is measured as a function of the detuning. The result is shown in figure 4. From a fit we extract a heating rate of 0.22 ± 0.07 quanta ms^{-1}, which is in fair agreement with the previous measurement.

4. Conclusion

We have demonstrated a technique to measure the absolute temperature of a single ion and its heating rate by measuring its spatial probability distribution in the trap. The high resolution image of the ion obtained by using our parabolic mirror as imaging tool allows us to measure temperature close to the Doppler limit, indicating the potential to perform thermometry below the Doppler limit. This would be of particular interest for measuring

[6] This estimate is an absolute lower limit for our experimental parameters, assuming that the Poissonian noise in image acquisition is negligible compared to uncertainties of PSF and magnification estimates.

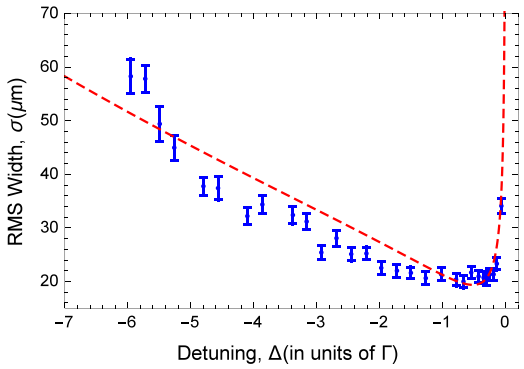

Figure 4. Image rms width along horizontal direction σ as a function of detuning Δ. The cooling beam power is fixed at a value corresponding to the on-resonant Rabi frequency (Ω) of 0.2 Γ. Error bars represent the uncertainty of the image width obtained by fitting a Gaussian to the camera images. The dashed (red) line represents a fit to the model with free fit parameters as in figure 3. The heating rate ζ obtained by the fit is 0.22 $\pm$ 0.07 quanta ms^{-1}.

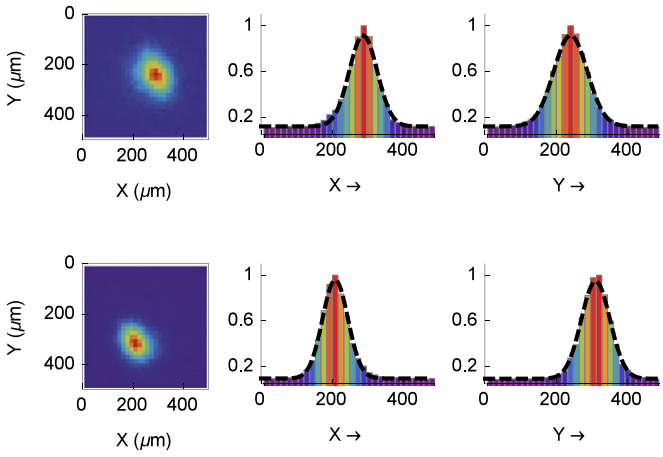

Figure A1. (Left) Images recorded on the EM-CCD camera for two positions of the ion, displaced in the by 635(2) nm in the x direction and 665(2) nm in the y direction. (Middle) Row scan of the images. Dashed line represents Gaussian fit function used to determine the x centers. (Right) Column scan of the images and the corresponding fit functions used to determine the y centers. The difference in the center position between the two images is 74.6 $\pm$ 1.8 μm and 72.5 $\pm$ 1.8 μm for x and y directions, respectively.

the temperature of an EIT cooled ion. The feasibility of imaging EIT cooled atoms using photons scattered off the cooling beams has been demonstrated recently [29].

We have also measured the heating rate in our trap, while the ion is constantly maintained in a thermal equilibrium. Therefore, this technique might be useful for traps exhibiting high anharmonicity or temperature dependent heating rates.

Acknowledgments

GL acknowledges financial support from the European Research Council (ERC) via the Advanced Grant 'PACART'. BS acknowledges support from the Alexander von Humboldt foundation.

Appendix A. Magnification calibration

To calibrate the magnification of the imaging system, we move the ion in the lateral direction using the piezo stage, and record the images on the camera as shown in figure A1. By comparing the image shift to the object (ion) displacement, we determine the magnification of our imaging system to be $M_x = 118(3)$ in the horizontal direction, and $M_y = 109(3)$ in the vertical direction. The magnification along the trap axes is $M = \sqrt{(M_x^2 + M_y^2)/2} = 113(2)$.

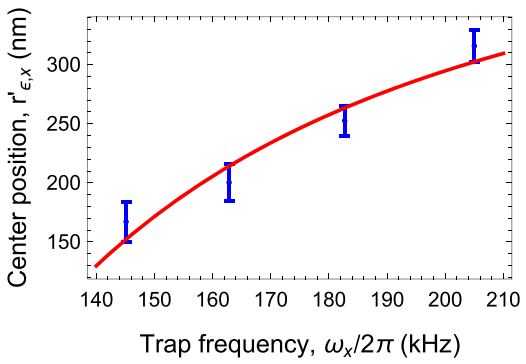

Figure B1. Mean x-position of the ion determined from its image on the EM-CCD chip as a function of the trap frequency in x direction. The origin of the coordinate system is arbitrarily chosen, and the ion x-position for each data point is measured by a Gaussian fit. The solid (red) line represents a fit of the measured points to the function $r'_{\epsilon,x}(\omega_x) = x_0 + \epsilon_x(Q/m\omega_x^2)$, where x_0 is the node of the pseudo-potential of the trap in this coordinate system. The free parameters determined from the fit are $x_0 = 453 \pm 38$ nm and $\epsilon_x = -0.45 \pm 0.08$ V m^{-1}.

Appendix B. Influence of excess micromotion

Stray electric fields cause excess micromotion which further broadens the spatial width of the ion wavefunction. Since our fit model does not include the micromotion effects, it is necessary to well compensate it in order to prevent any systematic errors. We use four auxiliary electrodes supplied with DC voltages that produce compensation fields to minimize micromotion.

Below, we present an estimate of the residual amplitude of excess micromotion that we typically have in our experiment after compensation. The motion of an ion in an RF trap in the presence of a stray electric field ϵ_k obeys the in-homogeneous Mathieu equation [30]. In adiabatic approximation, this motion is given by

$$r_k(t) \approx [r_{0,k}\cos(\omega_k t + \phi_k)]\left(1 + \frac{q_k}{2}\cos(\Omega_{\mathrm{RF}}t)\right) + r_{\epsilon,k} + \frac{q_k r_{\epsilon,k}}{2}\cos(\Omega_{\mathrm{RF}}t), \tag{B.1}$$

where $r_k\,(k = x, y, z)$ represents the ion position in each spatial dimension, and $\omega_k = (\Omega_{\mathrm{RF}}/2)\sqrt{a_k + q_k^2/2}$ is the secular trap frequency. Ω_{RF} is RF frequency which is $2\pi \cdot 5.2$ MHz in our experiment. a_k and q_k are the trapping parameters with $a_k \approx 0$ by design in our trap, which leads to $\{q_x, q_y, q_z\} \approx \{0.11, 0.11, 0.21\}$ for our operating trap frequency. $r_{0,k}$ is the amplitude of secular motion, and $r_{\epsilon,k}$ is the shift in the position of the ion due to a stray field from the node of the pseudo-potential. The last term in equation (B.1) represents the broadening due to excess micromotion.

The shift due to a static electric field ϵ_k is $r_{\epsilon,k} = (Q/m)(\epsilon_k/\omega_k^2)$ with ion charge Q and mass m. Using our imaging setup we measure this shift in x direction while varying the secular frequency ω_x (see figure B1). We determine the stray electric field from a fit to be -0.45 ± 0.08 V m^{-1}. At our operating trap frequency this would result in a shift of $r_{\epsilon,x} = 150 \pm 27$ nm. We can now determine the amplitude of excess micromotion to be 8.25 ± 1.48 nm. Since this is small compared to the lowest measured rms ion width of 166 nm in our experiment, it appears reasonable to neglect the excess micromotion contribution in our theoretical model.

Appendix C. Imaging PSF

We simulate intensity distribution of a radially polarized doughnut mode focused by our parabolic mirror, including the interferometrically measured aberrations by a generalization of the method presented in [31]. We obtain a FWHM width of the intensity distribution of 148nm for our wavelength. Including the magnification M of our imaging system, this translates to an expected PSF 7.1 μm at the EMCCD camera.

Although also extractable from the fits presented in section 3, we give an independent estimate of the size of the PSF of our imaging system as a consistency check. We generate a collimated radially polarized doughnut beam at the wavelength of the $P_{1/2} \rightarrow S_{1/2}$ transition at 370 nm wavelength as described e.g. in [32]. This mode is focused by the parabolic mirror. The rediverging beam is collimated again by the paraboloid and also imaged onto the EM-CCD camera. It thus passes the same optical elements as the fluorescence photons detected during the temperature measurements. The rms width of the image on the EM-CCD chip is determined by 1D Gaussian fits as shown in figure C1, yielding a width of $\sigma_{\mathrm{PSF}} = 12.3 \pm 0.5$ μm and 16.3 ± 0.5 μm for the horizontal and vertical direction, respectively.

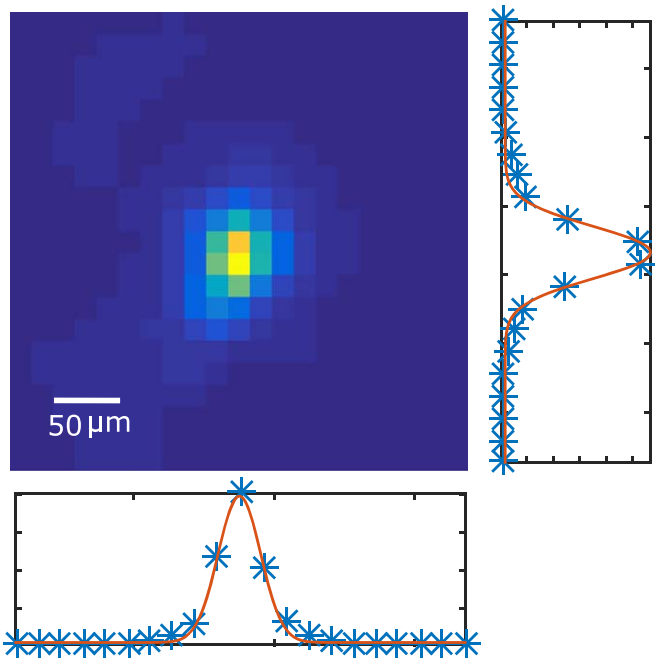

Figure C1. Imaging PSF measured with a radially polarized doughnut beam. The plots show the row and column projections of the recorded image, and the solid red line is Gaussian fit. The rms width is determined from the fit to be 12.3 ± 0.5 μm in the horizontal direction, and 16.3 ± 0.5 μm in the vertical direction.

The σ_{PSF} extracted from these measurements is also influenced by residual aberrations stemming from the optical elements used for preparing the doughnut beam. Moreover, this beam is reflected twice at the surface of the parabolic mirror. Thus, aberrations due to a non-perfect parabolic shape of the mirror [27, 32] are imprinted twice onto this beam. The phase front of the fluorescence photons emitted by the ion carries these aberrations only once. Furthermore, the spatial mode of the laser used in that measurement is not the same as the average spatial emission pattern of a $^{174}\mathrm{Yb}^{+}$ ion emitting photons on the $P_{1/2} \rightarrow S_{1/2}$ transition. After collimation by the parabolic mirror, the intensity pattern of the ion's fluorescence is of Lorentzian shape [26]. Therefore, the width of the PSF obtained in this measurement can be considered as an upper bound for σ_{PSF} in the temperature measurements.

Appendix D. Determination of the Rabi frequency

In order to determine the temperature of the ion from the image size, it is essential to precisely measure the on-resonance Rabi frequency Ω. We measure the effective Rabi frequency Ω' by performing a Hanbury–Brown–Twiss type experiment on the fluorescence photons. The detuning of the cooling beam is fixed at $\Delta = -\Gamma/2$. The power of the cooling beam, as measured by a power meter (Ophir Nova II), is fixed at a calibration value of $P = 50\ \mu$W. This value is chosen such that $\Omega' \gg \Delta$, which makes it possible to observe Rabi oscillations in $g^{(2)}$ measurement within the decay time. The on-resonance Rabi frequency is then determined from Ω' and Δ, $\Omega = \sqrt{\Omega'^2 - (\Gamma/2)^2} = 435(2)\,\mu\mathrm{s}^{-1}$.

The fluorescent light from the ion is split using a 50/50 beam splitter, and detected using two Photo-Multiplier Tubes PMT-A and PMT-B. A Time-to-Digital Converter is used to measure a Start–Stop correlation histogram between the PMT clicks, with a timing resolution of 161 ps. The normalized correlation function ($g^{(2)}(\tau)$) shown in figure D1 oscillates with a period that corresponds to the Rabi frequency. Since $\Omega \propto \sqrt{P}$, for subsequent measurements we determine Ω by measuring the cooling beam power P.

ORCID iDs

Markus Sondermann https://orcid.org/0000-0001-7913-6370
Gerd Leuchs https://orcid.org/0000-0003-1967-2766

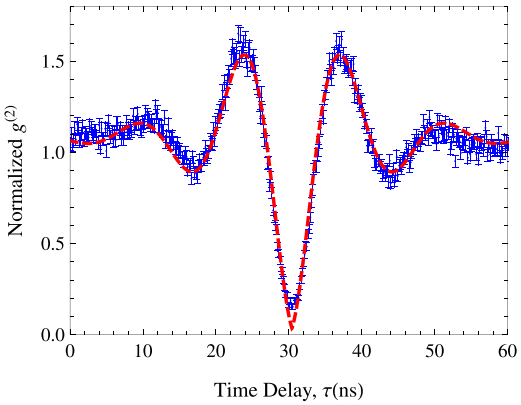

Figure D1. Normalized second order auto-correlation function of the ion fluorescence for the cooling beam power of $P = 50\ \mu$W. The delay in the minimum of $g^{(2)}$ is a result of an electronic delay between the detection events registered by PMT-A and PMT-B. The Rabi Frequency Ω' is determined from a fit of the measured points to a function of the form $g^{(2)}(\tau) = bg - A\left(\mathrm{Cos}^2\left[\frac{\Omega'}{2}(t - t_0)\right] - \frac{1}{2}\right)e^{\frac{-|t-t_0|}{\tau}}$. The resulting parameters from the fit are: $bg = 1.08(0), A = 2.09(3)$, $\Omega' = 0.439(2)\,\mu\mathrm{s}^{-1}$, $t_0 = 30.4(0)$ ns, and $\tau = 8.16(16)$ ns.

References

[1] Gibble K and Chu S 1993 *Phys. Rev. Lett.* **70** 1771–4
[2] Ludlow A D, Boyd M M, Ye J, Peik E and Schmidt P O 2015 *Rev. Mod. Phys.* **87** 637–701
[3] Cronin A D, Schmiedmayer J and Pritchard D E 2009 *Rev. Mod. Phys.* **81** 1051–129
[4] Bloch I, Dalibard J and Zwerger W 2008 *Rev. Mod. Phys.* **80** 885–964
[5] Häffner H, Roos C and Blatt R 2008 *Phys. Rep.* **469** 155–203
[6] Saffman M, Walker T G and Mølmer K 2010 *Rev. Mod. Phys.* **82** 2313–63
[7] Diedrich F, Bergquist J C, Itano W M and Wineland D J 1989 *Phys. Rev. Lett.* **62** 403–6
[8] Roos C, Zeiger T, Rohde H, Nägerl H C, Eschner J, Leibfried D, Schmidt-Kaler F and Blatt R 1999 *Phys. Rev. Lett.* **83** 4713–6
[9] Monroe C, Meekhof D M, King B E, Jefferts S R, Itano W M, Wineland D J and Gould P 1995 *Phys. Rev. Lett.* **75** 4011–4
[10] Roos C F, Leibfried D, Mundt A, Schmidt-Kaler F, Eschner J and Blatt R 2000 *Phys. Rev. Lett.* **85** 5547–50
[11] Wineland D J and Itano W M 1979 *Phys. Rev.* A **20** 1521–40
[12] Wineland D and Itano W M 1981 *Phys. Lett.* A **82** 75–8
[13] Dicke R H 1953 *Phys. Rev.* **89** 472–3
[14] Itano W M, Bergquist J C, Hulet R G and Wineland D J 1988 *Phys. Scr.* **1988** 79
[15] Blinov B B, R N Kohn J, Madsen M J, Maunz P, Moehring D L and Monroe C 2006 *J. Opt. Soc. Am.* B **23** 1170–3
[16] Norton B G, Streed E W, Petrasiunas M J, Jechow A and Kielpinski D 2011 *New J. Phys.* **13** 113022
[17] Knünz S, Herrmann M, Batteiger V, Saathoff G, Hänsch T W and Udem T 2012 *Phys. Rev.* A **85** 023427
[18] Rajagopal V, Marler J P, Kokish M G and Odom B C 2016 *Eur. J. Mass Spectrom.* **22** 1–7
[19] Maiwald R, Golla A, Fischer M, Bader M, Heugel S, Chalopin B, Sondermann M and Leuchs G 2012 *Phys. Rev.* A **86** 043431
[20] Slodička L, Hétet G, Röck N, Gerber S, Schindler P, Kumph M, Hennrich M and Blatt R 2012 *Phys. Rev.* A **85** 043401
[21] Deslauriers L, Olmschenk S, Stick D, Hensinger W K, Sterk J and Monroe C 2006 *Phys. Rev. Lett.* **97** 103007
[22] Brownnutt M, Kumph M, Rabl P and Blatt R 2015 *Rev. Mod. Phys.* **87** 1419–82
[23] Epstein R J *et al* 2007 *Phys. Rev.* A **76** 033411
[24] Boldin I A, Kraft A and Wunderlich C 2018 *Phys. Rev. Lett.* **120** 023201
[25] Leibfried D, Blatt R, Monroe C and Wineland D 2003 *Rev. Mod. Phys.* **75** 281–324
[26] Maiwald R, Leibfried D, Britton J, Bergquist J C, Leuchs G and Wineland D J 2009 *Nat. Phys.* **5** 551–4
[27] Leuchs G, Mantel K, Berger A, Konermann H, Sondermann M, Peschel U, Lindlein N and Schwider J 2008 *Appl. Opt.* **47** 5570–84
[28] Cirac J I, Garay L J, Blatt R, Parkins A S and Zoller P 1994 *Phys. Rev.* A **49** 421–32
[29] Haller E, Hudson J, Kelly A, Cotta D A, Peaudecerf B, Bruce G D and Kuhr S 2015 *Nat. Phys.* **11** 738
[30] Gloger T F, Kaufmann P, Kaufmann D, Baig M T, Collath T, Johanning M and Wunderlich C 2015 *Phys. Rev.* A **92** 043421
[31] Richards B and Wolf E 1959 *Proc. R. Soc.* A **253** 358–79
[32] Alber L, Fischer M, Bader M, Mantel K, Sondermann M and Leuchs G 2017 *J. Eur. Opt. Soc.-Rapid Publ.* **13** 14